Research on Engineering Structures & Materials
www.jresm.org
MIM Research Group

Research Article

Optimization of wear behavior in Ti-6Al-4V hybrid nanocomposites reinforced with TiC, ZrO_2, and graphite using friction stir processing

Allwyn Kingsly Gladston J [1,a], Chunduri Lavanya [2,b], Brundha B.A [3,c], Sellamuthu P [4,d], Suresh M [4,e], Mayakannan S [*5,6,f]

[1]*Department of Mechanical Engineering, SCAD College of Engineering and Technology, SCAD Nagar, Cheranmahadevi, Tirunelveli, Tamilnadu, India*
[2]*Department of Computer Science and Engineering, Koneru Lakshmaiah Education Foundation, Guntur, Andhra Pradesh, India*
[3]*Department of Chemistry, Vel Tech High Tech Dr. Rangarajan Dr. Sakunthala Engineering College, Tamil Nadu, India*
[4]*Department of Mechanical Engineering, Vinayaka Mission's Kirupananda Variyar Engineering College (VMRF -Deemed to be University), Salem, Tamilnadu, India*
[5]*Department of Mechanical Engineering, Saveetha School of Engineering, Saveetha Institute of Medical and Technical Sciences, SIMATS, Chennai, Tamil Nadu, India*
[6]*Department of Mechanical Engineering, Rathinam Technical Campus, Coimbatore, Tamilnadu, India*

Article Info

Article History:

Received 13 Feb 2025

Accepted 16 July 2025

Keywords:

Pin on disc;
Velocity;
Optimization;
Wear;
Load;
Metal matrix composites

Abstract

A hybrid nanocomposite surface layer was fabricated on Ti-6Al-4V alloy via friction stir processing (FSP) using titanium carbide (TiC), zirconium oxide (ZrO_2), and graphite (Gr) in varied weight ratios. Fixed-proportion mixtures were packed into 2.5 mm diameter, 3 mm deep holes, spaced 6 mm apart. Processing was carried out at a 3° tool tilt, 750 rpm rotational speed, and 20 mm/min traverse speed. Microstructural, macrostructural, hardness, and wear characteristics were examined. Scanning electron microscopy confirmed uniform dispersion of reinforcements, microstructural refinement, and enhanced wear resistance. Wear performance under dry sliding was optimized using central composite design (CCD) within response surface methodology (RSM). Pin-on-disc tests were conducted for composites with different reinforcement ratios. The hybrid nanocomposite achieved a hardness of 191 Hv, a 25.5 % improvement over the unreinforced FSPed alloy (149 Hv). Wear loss was strongly influenced by the TiC:ZrO_2 ratio, with graphite held constant. The conventional FSPed alloy showed a wear loss of 9.688 mm^3, whereas the optimal composition (20 % TiC–60 % ZrO_2–20 % Gr) achieved 2.9526 mm^3, a 49.6 % reduction. Under a 20 N load and 1 m/s sliding velocity, RSM identified ZrO_2 content (60 %) as the most significant factor. The regression model produced R^2 = 0.9955, predicted R^2 = 0.9501, and a maximum error < 2.2 %, confirming predictive reliability. Enhanced wear resistance is attributed to strong matrix–reinforcement bonding and graphite's lubricating action, which reduces shear stress. The results demonstrate the synergistic role of ceramic reinforcements and solid lubricants in developing cost-effective, high-performance Ti-based composites for demanding tribological applications.

*Corresponding author: kannanarchieves@gmail.com
[a]orcid.org/0009-0009-0683-2530; [b]orcid.org/0000-0003-4791-7441; [c]orcid.org/0000-0002-1231-7713; [d]orcid.org/0000-0001-8591-4343, [e]orcid.org/0000-0002-8610-995X, [f]orcid.org/0000-0002-3463-1965
DOI: http://dx.doi.org/10.17515/resm2025-679me0213rs

1. Introduction

Nowadays, engineers are always on the lookout for new, novel materials that are strong yet lightweight for use in product design. The end consequence is that alloys take the place of more conventional materials. Friction Stir Processing (FSP) has emerged as a transformative technique for enhancing the mechanical and wear properties of Ti-6Al-4V alloys, particularly in aerospace and marine applications. FSP offers a solid-state, eco-friendly approach to refine microstructures, introduce reinforcements, and tailor surface characteristics. Ti–6Al–4V alloy was machined using powder mixed EDM (PMEDM) with Graphite and TiO_2 powders in kerosene. The study evaluated effects on metal removal rate (MRR), surface integrity, surface roughness (SR), and tool wear, revealing that TiO_2 powder achieved higher MRR and less tool wear related to graphite. SEM images were used to assess surface morphology [1]. This interface enhanced microhardness and abrasion resistance, with performance improvements attributed to the smooth Ti-TiN bond [2]. Broad BCC phases and a dendritic microstructure were observed, showing Plasma Transferred Arc (PTA) effectiveness in alloying and doubling wear resistance compared to the untreated substrate [3]. Polymer gears made from pristine PAEK and MWCNT-reinforced composites were tested at various speeds and torques. Functionalized MWCNTs enhanced thermal resistance, wear performance, and surface finish, showing suitability for dynamic, high-load gear applications [4]. This study optimizes Friction Stir Welding (FSW) parameters for AA8090 aluminum-lithium alloy using a customized VMC setup. Using Central Composite Design (CCD), optimal UTS and % elongation were achieved at 1428 rpm, 36.4 mm/min, and 1.5° tilt. Significant interactions affected UTS, while % elongation remained unaffected. Microstructure, hardness, and fractography confirmed joint quality comparable to the base metal [5].

FSW of titanium alloy was conducted using a liquid-cooled Ni superalloy tool. The cooling system maintained the tool's temperature, resulting in FSW joints with microstructures and mechanical strength higher than the base material, indicating the efficacy of liquid cooling in FSW of titanium alloys [6]. The Ti-6Al-4V composite layer displayed a fully β-transformed microstructure, with improvements in hardness and wear resistance over two times greater than the base metal. Post-FSP heat treatment slightly reduced hardness but significantly improved impact toughness [7]. Multi-pass FSP reduced particle size and increased uniformity, enhancing the mechanical properties and wear resistance of the composites. Finite Element Analysis (FEA) aligned closely with experimental results, supporting the effectiveness of FSP for AMM enhancement [8]. Enhanced microhardness, wear resistance, and impact toughness were observed, attributed to microstructure refinement, martensite formation, and dispersion strengthening through Zener pinning and particle-stimulated nucleation [9]. FSP of rolled Ti-6Al-4V alloy sheets achieved a fully lamellar microstructure, with superplastic elongation up to 553% at 875°C due to dynamic globalization and boundary sliding mechanisms, enhancing thermal-mechanical stability [10].

FSP was used to harden Ti-6Al-4V produced by wire-feed electron beam additive manufacturing, with findings showing that increased axial load forms a β-transformed structure but reduces strength, while FSP improved tensile strength by up to 69% [11]. Structure formation in the stir zone of 3D-printed Ti-6Al-4V was studied during FSP, showing different adhesion zones depending on processing direction relative to wall growth, influenced by the tool's adhesion-diffusion transfer [12]. Al2024-T3 and Ti-6Al-4V were lap jointed by friction stir welding (FSW), exploring the impact of tool profile and span on interface microstructural and tensile-shear properties. Half spherical pin tips produced a sharp, semi-coherent interface, while longer flat tips led to thicker multi-layered intermetallic compounds, affecting joint strength and ductility [13]. Hot rolled TC4 titanium alloy plates were welded by FSW, with tool wear analyzed through mass loss, 3D imaging, and SEM. Results showed wear types like mechanical, abrasive, and oxidative, correlating with welding distance; severe tool wear polluted joints and formed defects [14]. FSW of Ti-6Al-4V examined the impact of shoulder diameter, tool geometry, and speeds on joint properties. Optimal parameters yielded a defect-free joint with tensile strength of 809.8 MPa, with taper cylindrical pins enhancing frictional heat and stirring action [15]. Lightweight aerospace components were manufactured using solid-state joining methods, including friction welding and diffusion bonding, avoiding hot cracking and achieving high-quality joints. These methods mixed materials mechanically at elevated temperatures for cost-effective, durable structures [16]. FSW was used

for Ti-6Al-4V sheets, with machine learning (ML) models like regression and neural networks discussed to optimize welding conditions and predict flaws. The study highlighted ML's role in improving weld quality by predicting microstructural changes and potential fracture failures [17]. Performance of friction-welded Ti6Al4V rods was evaluated under various speeds and pressures, with optimal tensile strength of 1040 MPa at 1900 RPM and 80 MPa. Fine recrystallized grains and martensitic structures were observed, and hardness was higher across all welded zones related to the base material [18]. Optimization of FSW factors for an AA6061-based composite with 6% ZrO_2 and 2% graphite aimed to enhance tensile strength and hardness. Using Box-Behnken design and desirability functions, an optimal UTS of 190 MPa and hardness of 45 HRB were achieved at 46.88 mm/min, 808 rpm and 5.23 kN axial load [19].

Ti-6Al-4V titanium alloy's wear resistance was enhanced through laser surface alloying with Ni-coated graphite (G@Ni), creating a self-lubricating composite coating. The coating's hardness was four times that of the substrate, while its wear resistance improved 8.53 times due to the TiC hard phase and residual graphite reducing friction [20]. Diamond and diamond/graphite composite coatings on TC4 alloy were produced by high-frequency induction heating, showing good metallurgical bonding. In-situ TiC and ZrC particles in the composite improved the wear resistance, though free graphite slightly weakened the coating's structure; abrasive wear was the main wear mechanism observed [21]. Laser surface alloying with G@Ni on Ti-6Al-4V enhanced wear resistance by refining the microstructure at higher laser scanning speeds. At 15 mm/s, the coating exhibited the minimum wear weight loss owing to its high microhardness and dense structure, highlighting the impact of scan speed on coating behaviour [22]. The Friction Stir Processing (FSP) parameters—specifically 750 rpm tool rotational speed and 20 mm/min traverse speed is based on achieving effective reinforcement dispersion, defect-free surface composites, and optimal microstructural refinement.

Despite the advances, there is limited research on hybrid reinforcement systems that combine hard ceramic particles (like TiC and ZrO_2) with solid lubricants (like graphite) in Ti-6Al-4V via multi-pass FSP. Moreover, the effect of micro/nano hybrid particle distribution and their synergistic mechanisms—such as load sharing, lubrication film formation, and Zener pinning—are not comprehensively addressed. Prior works have also rarely integrated statistical optimization (e.g., RSM-CCD) with empirical validation across wear, hardness, and microstructure metrics. This study addresses these gaps by developing a Ti-6Al-4V-based surface nanocomposite with TiC-ZrO_2-Graphite hybrid reinforcements using multi-pass FSP. The research evaluates the effect of reinforcement ratios on tribological behavior and applies RSM to optimize wear performance. Statistical validation, SEM/EDS analysis, and benchmarking with previous studies substantiate the performance gains and confirm the process repeatability.

2. Experimental Methodology

2.1. Material

The superiority of Ti-6Al-4V lies in its high temperature stability, outstanding corrosion resistance, and maximum strength-to-weight ratio. The alloy is needed as a matrix in FSP because it enhances mechanical properties, reduces porosity, and improves wear resistance in the processed area. Applications of FSP with Ti-6Al-4V include aerospace components, biomedical implants, and automotive parts where precision and durability are essential. FSP refines the microstructure, making the alloy suitable for high-stress environments and enhanced fatigue life. Consequently, it is chosen as the main component for making nanocomposites. The chemical arrangement of Ti-6Al-4V is shown in Table 1.

Table 1. The chemical arrangement of Ti-6Al-4V.

Element	Composition (wt%)
Al	5.8
V	3.9
Fe	0.40
O	0.20
C	0.08
N	0.05
H	0.015
Ti	Balance

Titanium Carbide (TiC) is important for its exceptional hardness and wear resistance, enhancing material durability. It is needed in FSP for applications like cutting tools and aerospace components where improved abrasion resistance and thermal stability are crucial. Zirconium Dioxide (ZrO_2) is vital for its excellent thermal stability and toughness, enhancing the strength and wear resistance of materials. It is used in applications like ceramic coatings and biomedical implants where improved durability and resistance to high temperatures are essential. Graphite is becoming more popular as a supplementary material for reinforcement due to its ability to enhance the tribological performance of composites in arid sliding circumstances. It generates a thin layer that obstructs metal contact, thereby reducing specific wear rate.

2.2. Optimization Using RSM

RSM is a statistical and mathematical framework that minimizes experimental effort while achieving optimal results for input variables and responses. By employing evaluative data, RSM will improve the experimental methodology. This study utilizes RSM to optimize the input factors (A, B, C) and the response variable (wear) by analyzing the interactions between them. In order to guarantee a total composition of 100% with respect to the quantity of ZrO_2 in the mixture, the surface hybrid nanocomposites under investigation were developed using a reinforcement mixture that contained a predetermined percentage of graphite particles (20%), a variable percentage of nano ZrO_2 (20–60%), and a corresponding percentage of TiC (20–60). The optimal values of TiC and graphite for the formulated ZrO_2 are presented in Table 2.

Table 2. A reinforcement mixture's combination ratio.

ZrO_2 (wt%)	TiC (wt%)	Gr (wt%)
20	60	20
40	40	20
60	20	20

The quadratic model shown in equation 1 forecasts the results in relation to the input factors. The experimental outcomes attained from Design Expert 11 produce the model coefficients.

$$Y_n = b + \sum b_i x_{in} + \sum b_{ii} x_{in}^2 + \sum b_{ij} x_{in} x_{jn} \quad (1)$$

The coefficients are represented by b, b_i, b_{ii}, and b_{ij} are constant coefficient, linear term coefficient, quadratic coefficient and interaction term coefficient, respectively, while the response is denoted by Yn. RSM implemented CCD with complete factorial. Six center points were employed to apply three input factors. The coded and real values, along with their respective ranges are illustrated in Table 3. Twenty experimental combinations are produced by a CCD with an $\alpha = 1$. The experimental observations are summarized in Table 4.

Table 3. Experimental input factors

S. No	Parameters	Symbols	Units	Level		
				-1	0	+1
1	ZrO_2	A	%	20	40	60
2	Load	B	N	25	35	45
3	Velocity	C	ms^{-1}	1	1.3	1.6

Table 4. Design of experiments using L20 Orthogonal array

Experiment No	A (%)	B (N)	C (ms)−1	Wear (mm^3)
1	40	25	1.3	8.50
2	40	35	1.3	9.16
3	60	45	1.6	7.69
4	60	25	1.6	6.35
5	20	45	1.6	8.25
6	40	35	1.3	9.21
7	20	25	1.6	6.93
8	40	35	1.3	9.10
9	40	35	1.3	9.19
10	20	35	1.3	7.35
11	60	25	1	6.11
12	20	45	1	8.14
13	40	35	1.3	9.23
14	40	45	1.3	10.08
15	20	25	1	6.52
16	40	35	1	8.92
17	40	35	1.3	9.00
18	40	35	1.5	9.45
19	60	35	1.3	6.61
20	60	45	1	7.17

2.3. Fabrication of Nanocomposite

The Ti-6Al-4V alloy was used as the matrix material, commercially obtainable in slabs with a thickness of 6 mm. The plates were trimmed to the necessary dimensions of 200 mm × 100 mm. The reinforcements used in this composite are nano-scale zirconium oxide, micro-scale titanium carbide, and graphite particles, with average diameters of 45 nm, 2.5 µm, and 5 µm, correspondingly. A brittle phase forms at the grain boundaries of the composite when the concentration drops below a particular point, because the grain boundaries are saturated with hard nano-ceramic particles. Due to a decrease in anchoring activity near the grain boundary, this mechanism weakens the material. The use of both nano and micro reinforcements was considered as a potential solution to this issue, as it would enhance binding strength and facilitate reinforcement dispersion. The Ti-6Al-4V alloyed surface exhibited 718 HV0.2 hardness, 2.2 times higher than the base material, and enhanced wear resistance due to solid solution strengthening and oxide film formation that improved tribological performance [23].

A selection of zigzag blind holes was established along the center of the Ti-6Al-4V plate, with an interval of 6 mm between them. The reinforcement powders (TiC, ZrO_2, and Gr) were manually packed into the perforations after being mixed with methanol in a variety of ratios, as shown in Table 5.

Table 5. Composition of various surface nano composites.

S. No	Sample code	Composition
1	S0	Basemetal Ti-6Al-4V
2	S1	80%TiC + 20 %Gr
3	S2	80% ZrO_2 + 20% Gr
4	S3	60%TiC+20%ZrO_2 + 20% Gr
5	S4	40%TiC+40%ZrO_2 + 20% Gr
6	S5	20%TiC+60%ZrO_2 + 20% Gr

Two unique instruments were utilized for FSP, one equipped with a probe and the other devoid of it. Both tools had a shoulder diameter of 18 mm and were made of strengthened high-speed steel. Figure 1(a) shows the dimension of the tool. Figure 1 (b) shows the experimental process of friction stir welding. This instrument used a probe-free capping run of FSP to seal the groove and prevent reinforcement particles from being ejected. The equipment that was equipped with the probe was used to do stir processing. Process parameters for FSP were as follows: 20 mm/min traversal speed, 750 rpm tool rotating speed [24], and a 3° tool tilt angle.

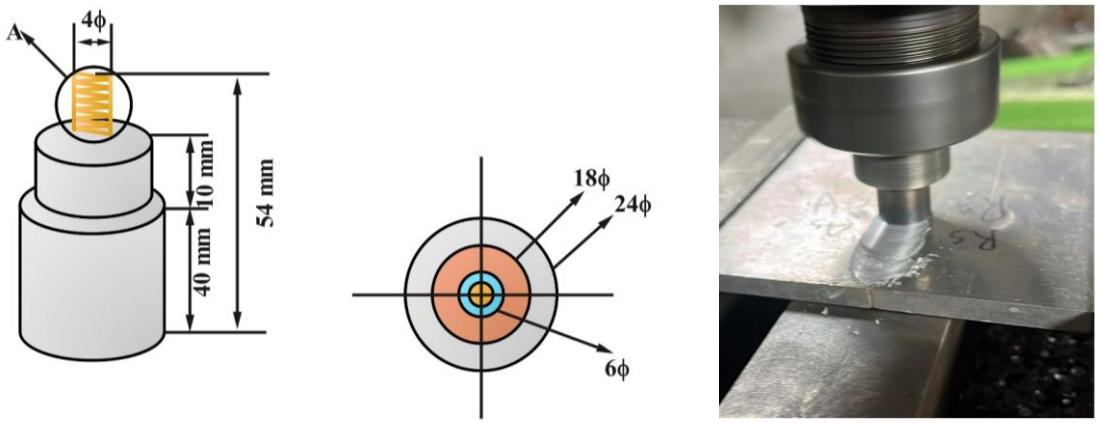

(a) (b)

Fig. 1. (a) Tool dimensions (b) friction stir welding machine

Three stirring frictions stir processing passes and one capping pass, with varying directions for each, were performed to achieve uniform particle distribution. The ideal reinforcement distribution in Ti-6Al-4V surface composites is achieved through the defined process parameters and circumstances. Figure 2 illustrates a representation of FSP. Figure 3 depicts the SEM analysis (a) Zirconium oxide (b) Titanium carbide (c) Graphite reinforcing particles utilized in composite fabrication. The friction stirs welding machine (Model: 2100 rpm, 11 kW, SPM/04, 30 kN) was utilized to do the friction stir processing.

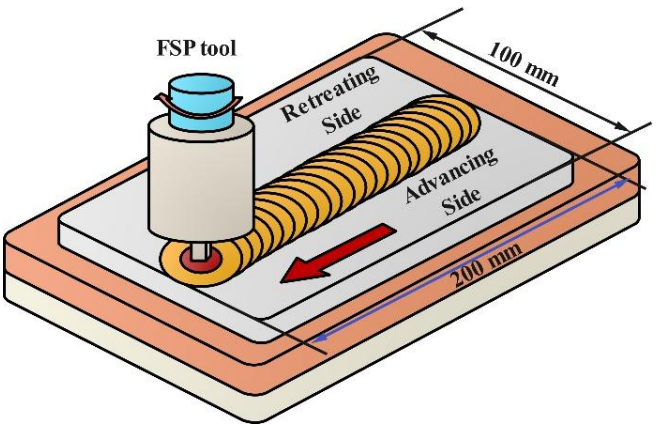

Fig. 2. Schematic view of friction stir welding

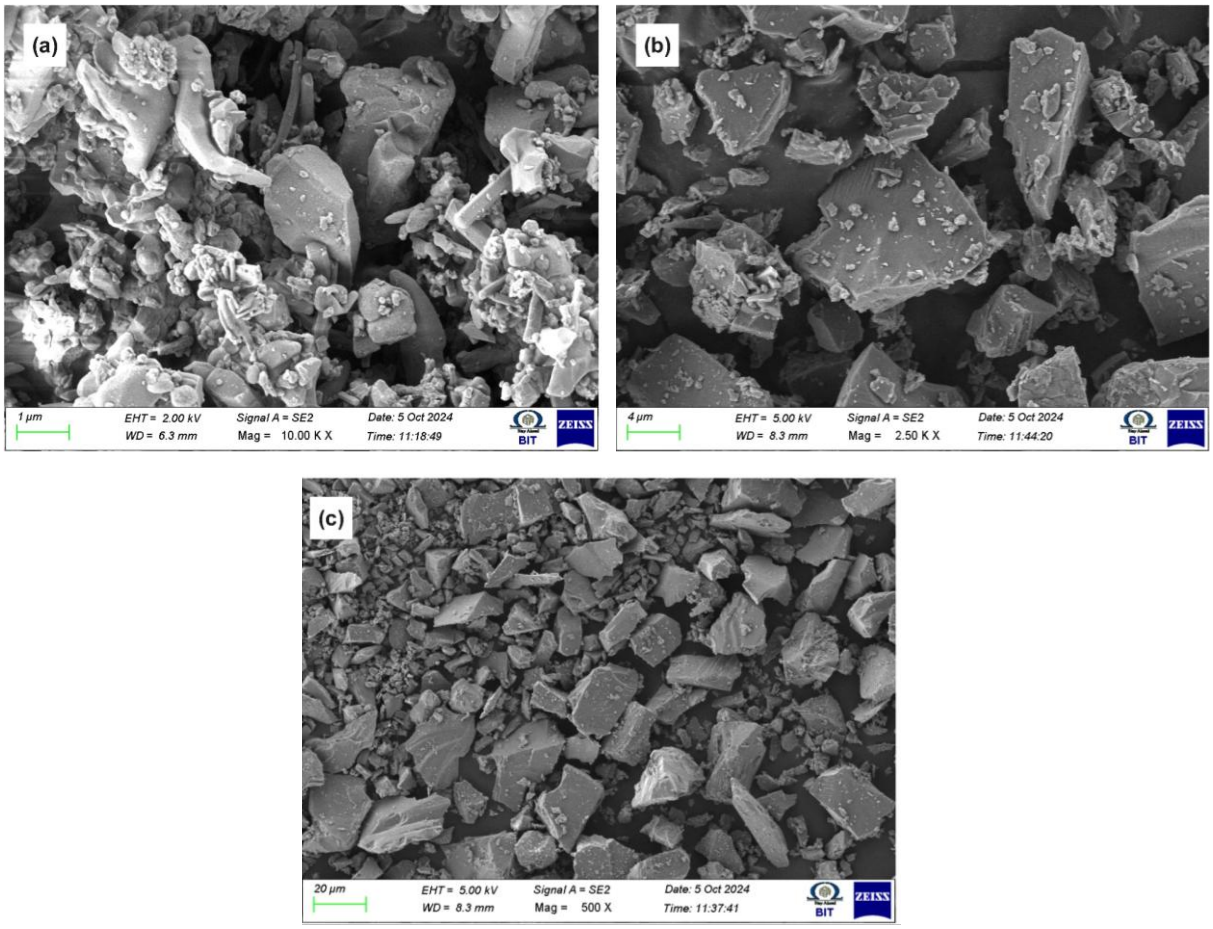

Fig. 3. (a) Zirconium oxide (b) titanium carbide (c) graphite reinforcement particles

2.4. Microstructural and Microhardness Analysis

A Vickers microhardness tester was used to conduct the microhardness evaluation under a force of 300 g for a duration of 15 seconds. In a cross-sectional view of the agitation zone, 1mm beneath the treated surface, the indent was measured between a parallel line at 1mm intervals.

Microstructural analyses were conducted on samples that were extracted from the surface nanocomposites. Macrostructure, microstructural characteristics, and microhardness were assessed within the nugget zone (NZ) by sectioning the samples perpendicular to the FSP direction.

A SEM with an energy dispersive X-ray spectrometer (EDS) (ZEISS) were utilized for microstructure analysis and elemental mapping. Following milling with abrasive sheets up to 2500 grit, the specimens were polished using diamond paste in a polishing machine and subsequently etched using Keller's solution. Macrostructures were analyzed using an optical microscope OM (Model: MIL-7100) manufactured by MEJI-Japan.

2.5. Wear Study

The pin-on-disc tests were conducted using a hardened EN31 steel disc (hardness: 62 HRC), commonly used in tribological studies. The disc had a surface roughness (Ra) of 0.25 µm, measured using a stylus profilometer, ensuring a consistent and controlled interface. In accord with ASTM-G99–17 standards, the wear behavior was evaluated under dry sliding conditions at 25 °C and 60% relative humidity using a DUCOM POD wear tester (Model: TR20-PHM-M1), as illustrated in figure 4(a). The wear test utilized CNC wire cut EDM to extract cylindrical pin samples from the center of the NZ, orientated vertically to the FSP track (figure 4(b)). The diameter and length of the pin was 6 mm respectively. The associated disc with a hardness of 62 HRC. The pin samples were measured with an accuracy of 0.1 mg utilizing an electronic balance (Make: SHIMADZU). Model: AY220, both before and after the experiment. The needles are purified with acetone and permitted to dry

following the end of each test in readiness for weight evaluation. The volume in cubic millimeters was derived from the measured weight loss for analysis. The worn specimens were exposed to a constant force of 20N at 1.5 m/s throughout the testing procedure. The SEM was utilized to analyze the corroded surfaces of the pin.

(a) (b)

Fig. 4. (a) Pin on Disc wear testing machine (b) wear test sample

3. Results and Discussion

3.1. Optimization

Design expert 13 evaluated the deterioration. The maximum to minimal wear volume ratio is 2.42, which suggests that no modification is required. The quadratic model is pertinent to the wear response, as seen by the fit summary. The results of the deterioration analysis of variance (ANOVA) are shown in Table 6. At the 95% confidence level, the model's p-value is less than 0.0001 and the F-value is 246.18. When the p-value is less than 0.05, it means that the model accepts ZrO_2, load, velocity, and the higher order of ZrO_2 as relevant input parameters. The regression coefficient (R^2), and adjusted R^2 are highly connected and almost equal to one. This demonstrates that the model aligns with empirical facts.

Table 6. ANOVA for wear

Source	Sum of Squares	df	Mean Square	F-value	p-value	
Model	27.76	9	3.08	246.18	< 0.0001	significant
A	1.06	1	1.06	84.82	< 0.0001	significant
B	4.79	1	4.79	382.17	< 0.0001	significant
C	0.3276	1	0.3276	26.15	0.0005	significant
AB	0.0364	1	0.0364	2.91	0.1189	not significant
AC	0.0072	1	0.0072	0.5746	0.4659	not significant
BC	0.0000	1	0.0000	0.0040	0.9509	not significant
A^2	12.99	1	12.99	1036.50	< 0.0001	significant
B^2	0.0515	1	0.0515	4.11	0.0702	not significant
C^2	0.0028	1	0.0028	0.2222	0.6475	not significant
Residual	0.1253	10	0.0125			
Lack of Fit	0.0886	5	0.0177	2.42	0.1776	not significant
Pure Error	0.0367	5	0.0073		R^2	0.9955
Cor Total	27.89	19	Mean	8.15	Adj. R^2	0.9915
Std. Dev.	0.1119		C.V. %	1.37	Pred. R^2	0.9501

While the regression model achieved a high coefficient of determination (R^2 = 0.9955), this value may reflect potential overfitting due to the limited number of experimental runs (n = 20) relative to the number of model terms. Although adjusted R^2 (0.9915) and predicted R^2 (0.9501) are closely aligned, suggesting reasonable generalizability, no formal cross-validation (e.g., k-fold or leave-one-out) was performed. This represents a limitation of the current model. Additionally, the wear prediction model was developed specifically for Ti-6Al-4V hybrid nanocomposites reinforced with TiC, ZrO_2, and graphite under dry sliding conditions. Its applicability to other alloys, reinforcement systems, or lubricated environments remains unverified. Future work should include cross-validation techniques and broader experimental designs to ensure robustness and wider applicability of the regression model.

The requisite precision value of 4 is substantially exceeded by the appropriate precision value of 50.5023. The value of 0.0177 indicates that the lack of fit is not as significant as is required. Equation (2) provides the precise formulation of the wear response equation.

$$\begin{aligned} Wear\ Resistance \\ &= +9.15 - 0.326\,A + 0.692\,B + 0.181\,C - 0.0675\,AB \\ &+ 0.03\,AC - 0.0025\,BC - 2.1732\,A^2 + 0.1368\,B^2 \\ &+ 0.03182\,C^2 \end{aligned} \tag{2}$$

Equation (2) indicates that the percentage of ZrO_2 and velocity significantly contribute to wear. A response surface graph was created using three pairs of input parameters to depict the correlation between the pairings and the wear response. Figure 5(a) illustrates the relationship between ZrO_2 and load, indicating that wear escalates with load, exhibiting a slight curve. Conversely, the wear associated with ZrO_2 demonstrates a parabolic relationship, increasing to a specific threshold before diminishing with the rise in ZrO_2 content. Figure 5(b) illustrates the correlation between ZrO_2 content and velocity, indicating that wear escalates linearly with velocity and exhibits a parabolic connection with ZrO_2 concentration. The graph (Figure 5(c)) depicting the relationship between load and velocity indicates a progressive linear rise in wear with velocity, accompanied by a minor curvature in relation to load.

The quadratic model is consistent with the actual data, as indicated by the ANOVA. As the P-value < 0.0001, the most important parameters are the percentage of ZrO_2 and the load. The response graph suggests that wear increases in a linear manner in proportion to the load. Wear increases with the percentage of ZrO_2 content at a constant strain until a specific threshold is reached, at which point it decreases. At a fixed velocity, wear escalates parabolically and diminishes with the percentage of ZrO_2. The wear escalates with an increase in load at the specified velocity.

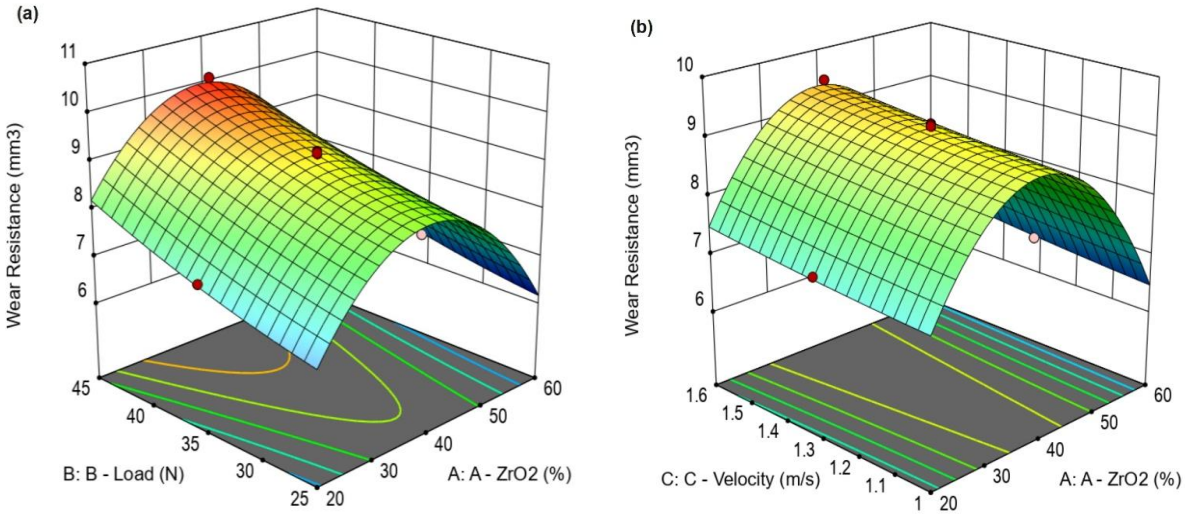

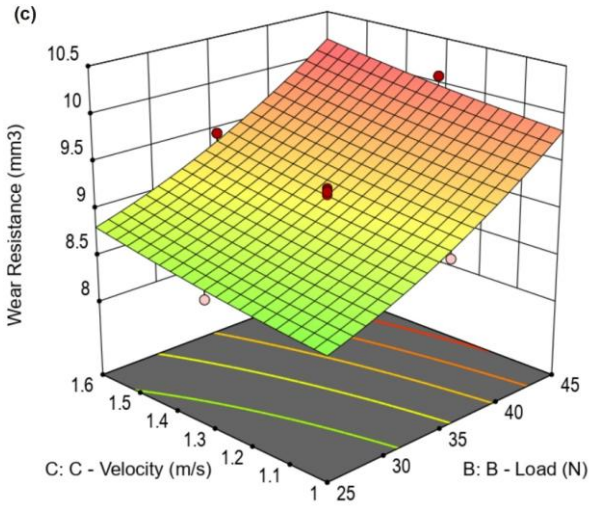

Fig. 5. RSM plot for the wear (a) A vs B, (b) A vs C, (c) B vs C.

3.2. Micro and Macro Structures

The FSP method was employed to produce hybrid nanocomposites with an Ti-6Al-4V surface that were free of defects. The reinforcement clusters' size, which was initially 2–3 μm during a single friction stir processing run, considerably decreased to 0.1–0.5 μm after three passes (Figure 6). The dimensions of the clusters reduced with the escalation of passages. Figure 7(a) illustrates the friction stir processing of the composite, characterized by a uniform surface free of defects. Figure 7(b) illustrates the macro image of hybridized composites, highlighting the cross-sectional image at nugget zone. The specimens have been processed flawlessly and are free of defects. The reinforcements are evenly distributed, as demonstrated by the analysis. The treated surface of the NZ was 18 mm, whereas the base was 6 mm. The overall elevation of the NZ, measuring 4.6 mm, exceeded that of the pin. The displacement of the plasticized material occurs as it traverses the tapered threaded pin. The shoulder friction necessitated the deployment of strengthening in the top section of the treated area. The coarse grains were more prevalent in the shoulder region compared to the pin-controlled region.

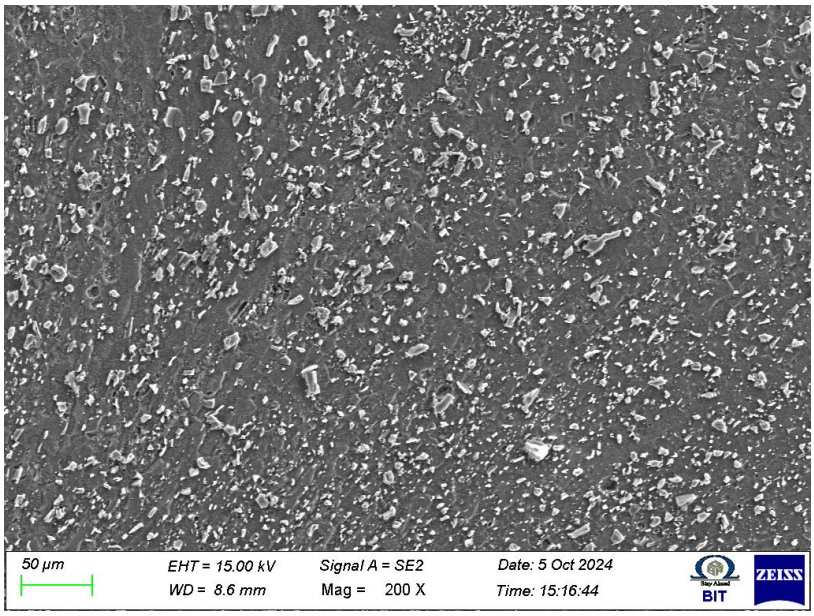

Fig. 6. Microstructural image of the stir zone

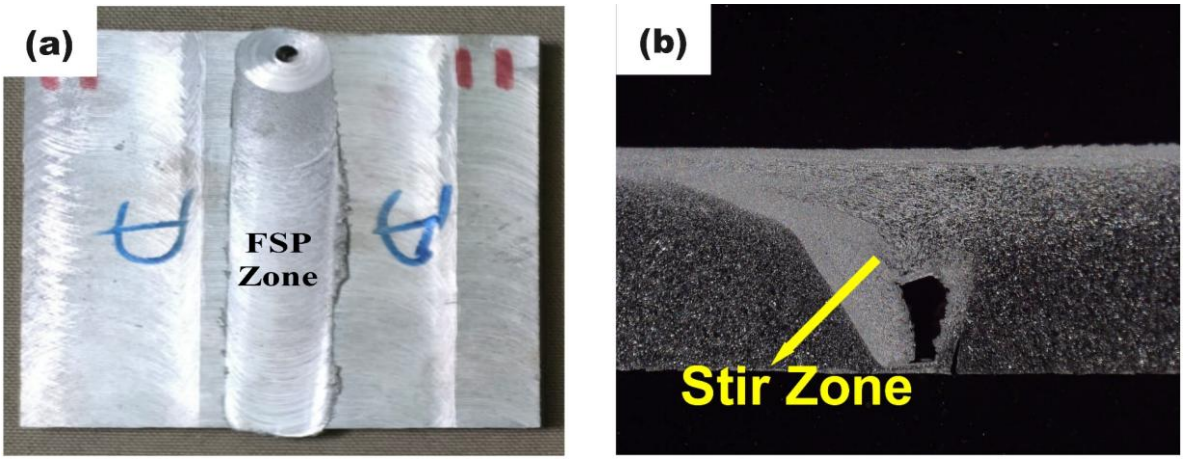

Fig.7. FSP zone of (a) Top view (b) cross-sectional view of macro image

Figures 8(a-b) present the SEM and EDS image of the surface hybridized nanocomposite sample that was manufactured, which contains 20%TiC, 60% ZrO_2, and 20% Gr. Both the visualization and the EDS picture show that the fabricated nanocomposite has reinforcements with the visualization allowing to identify specific particles.

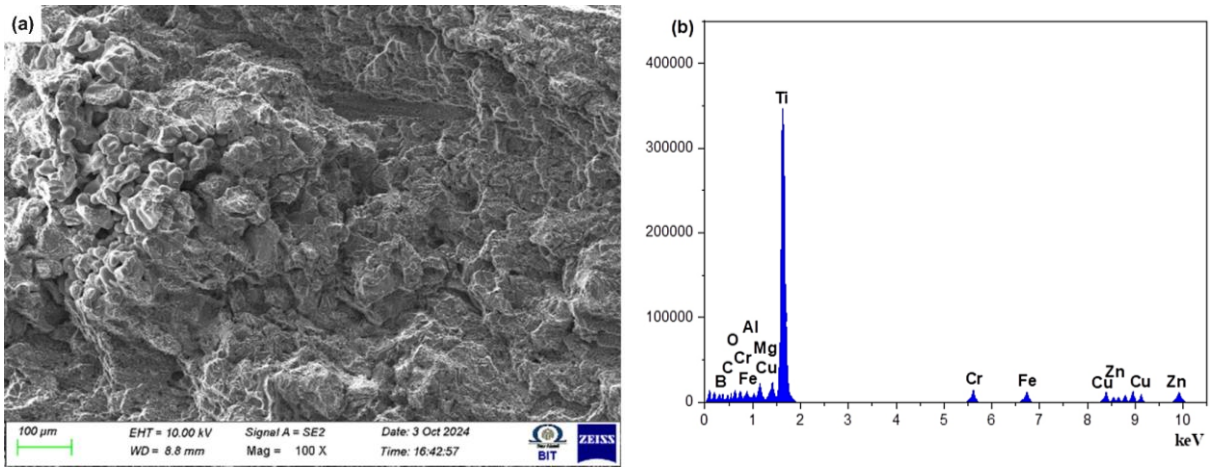

Fig. 8. (a) SEM image of S5 (b) EDS

Enough stirring in FSP ensures that the reinforcements are dispersed uniformly. The surface composite layer is formed by cohesively incorporating the reinforcing particles into the matrix. Because the processing direction changes with each iteration, the dispersion of particles for the advancing region and retreating region armies is comparable. When the Ti-6Al-4V under the shoulder blocks the stream of material, it reaches a standstill on the front side. In order to achieve a uniform distribution of reinforcements, the process orientation was changed with each iteration. Elements of SHNC 20%TiC + 60 %ZrO_2 + 20% Gr were mapped out to show where the carbon, boron, and oxide reinforcements were distributed (Figure 9).

Figure 9 (a) shows the SEM analysis of sample 5. In addition to elemental mapping, quantitative EDS analysis was performed at selected points in the nugget zone to confirm the presence and distribution of reinforcement elements (Figure 9b). Figure 9 (c) to (e) shows the dispersion of oxygen, aluminum and iron particles of sample 5. The EDS spectra indicated average compositions of ~18–22 wt% Zr, ~14–17 wt% C, and trace O in the reinforced zones, confirming the integration of ZrO_2 and graphite. Ti remained the dominant matrix element (~50–55 wt%), with Al and V detected within their base alloy ranges. These values corroborate the reinforcement ratios used and support successful incorporation without major compositional dilution or clustering. Minimal Fe contamination was observed, indicating negligible tool wear during FSP.

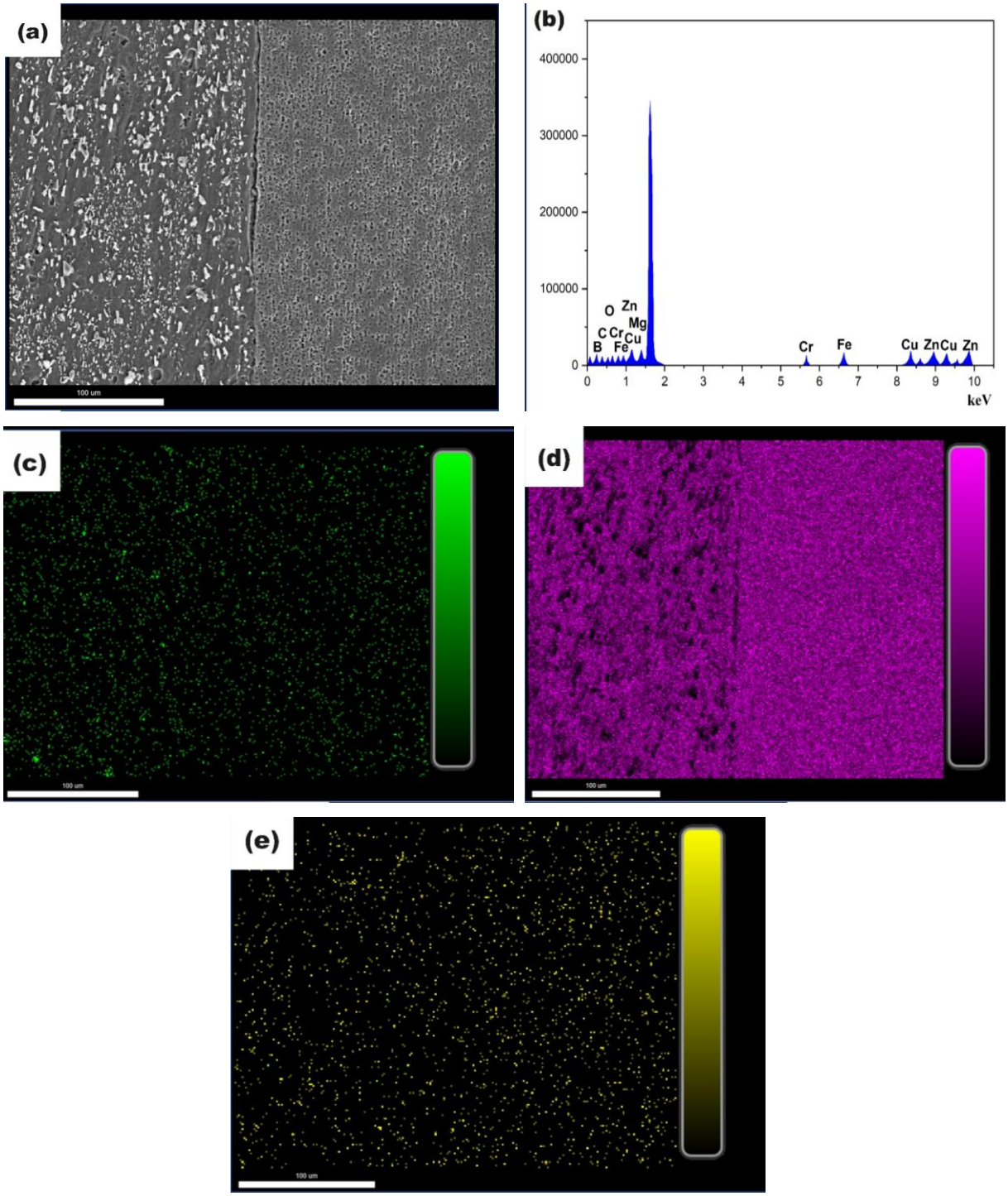

Fig. 9. (a) SEM (b) EDS, (c) oxygen dispersion of particles (d) aluminum dispersion of particles (e) iron dispersion of particles of elemental mapping analysis of sample 5

Due to the significant residual stress versus strain in the base alloy plate, the plastic deformation and flow of the primary friction stir passing pass are constrained. The base matrix becomes more ductile in subsequent iterations, which enhances the matrix's fluidity. The FSP passes were conducted in this study in a progressive manner, transitioning from a single capping pass to three stirring passes. The orientation of the passes was altered between each pass, and cooling intervals were not accommodated. Air is employed to cool the sample and its accompanying backplate. The heat produced during the initial pass preserves and softens the processing plate, therefore enhancing material flow and stirring action in the subsequent second and third passes. The reduction in cluster size and uniform allocation of reinforcements are confirmed by this action. Ultimate strength increased after three passes due to grain refinement, though four passes led to

coarser grains and a slight drop in strength, while wear resistance improved by 39% compared to the initial alloy [25].

The FSP tool pin was rotated for multiple revolutions, and the matrix underwent intensive plastic deformation. Thereafter, the angled tool was employed to shape the material at a specified plunge depth. The deformed matrix flows more rapidly than the rigid ceramic reinforcements, promoting the breakup of particle clusters and ensuring a uniform distribution in the NZ throughout repeated weld passes. Fragmentation results from the mechanical stress experienced by the brittle ceramic reinforcing particles during Friction Stir Processing (FSP). The micrographs of the samples that were subjected to three passes clearly demonstrate this. The base material's recrystallization temperature was exceeded during the FSP. When substantial plastic deformation and friction work together, they generate the necessary heat for dynamic recrystallization to take place. The high stacking fault energy of aluminum promotes dynamic recrystallization.

The FSP procedure resulted in the refinement of the surface composites, resulting in finer granules. The three-cycle friction stir technique, which included dynamic recrystallization, is to owing for this improvement. A fine-grained structure is achieved because the nano reinforcing components attach and inhibit grain development. The expansion of the grain boundary is impeded by the second phase elements as a result of Zener anchoring.

SEM image of the microstructure and energy dispersive spectroscopy (EDS) in the nugget zone of the samples with varying reinforcement ratios (TiC, ZrO2, Gr) of samples S0 to S5 are shown in Figure 10. There was no formation of new phases in the matrix due to the FSP technique. The reinforcement particles are dispersed evenly because the graphene particles in the mixing function as a oil and inhibit accumulation during process. SEM analysis revealed minimal voids with a 15% increase in microhardness at peak machining levels [26]. Due to the thermodynamic stability and inertness of titanium carbide to the Ti-6Al-4Vmatrix, the FSP process is devoid of any potentially harmful components. The micrograph indicates that the reinforcements and the matrix exhibit improved interfacial adhesion.

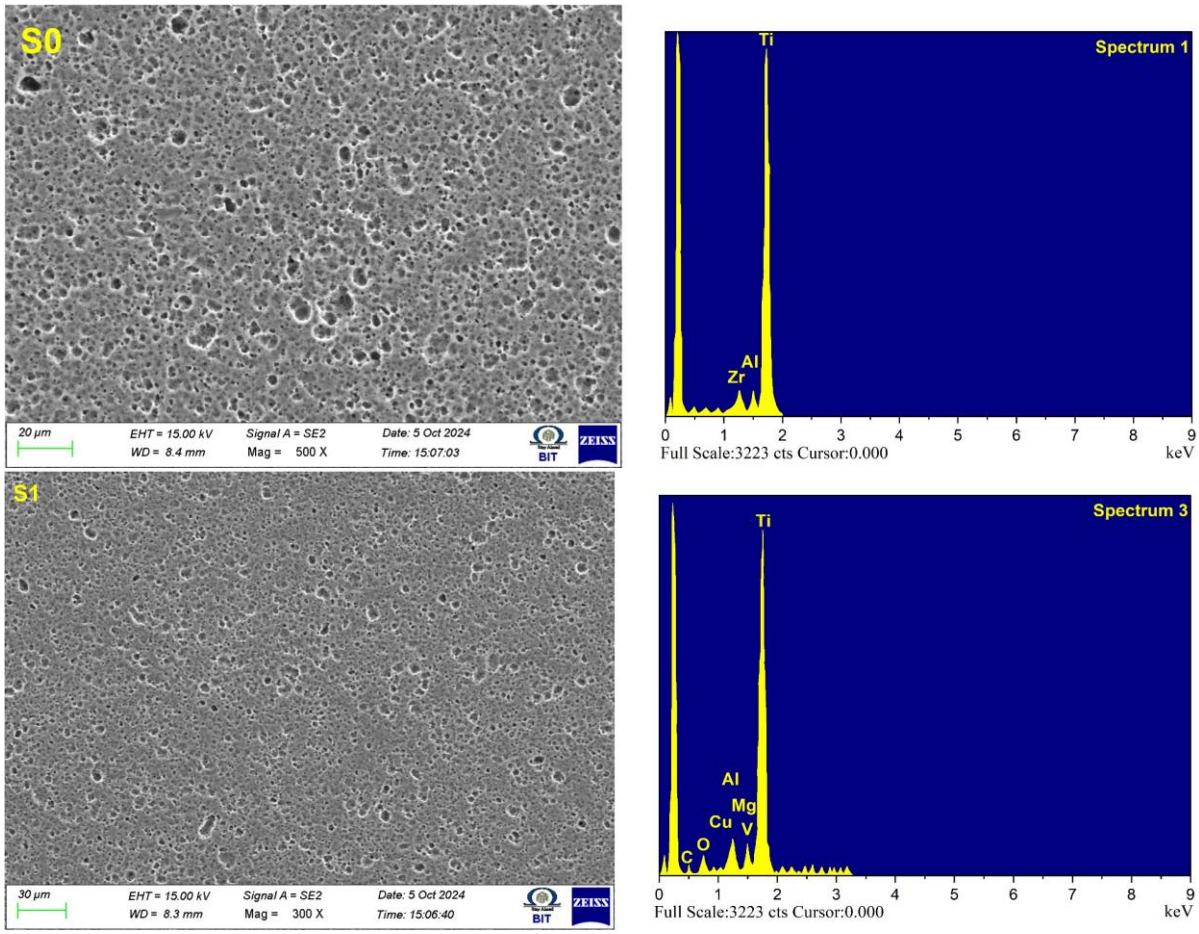

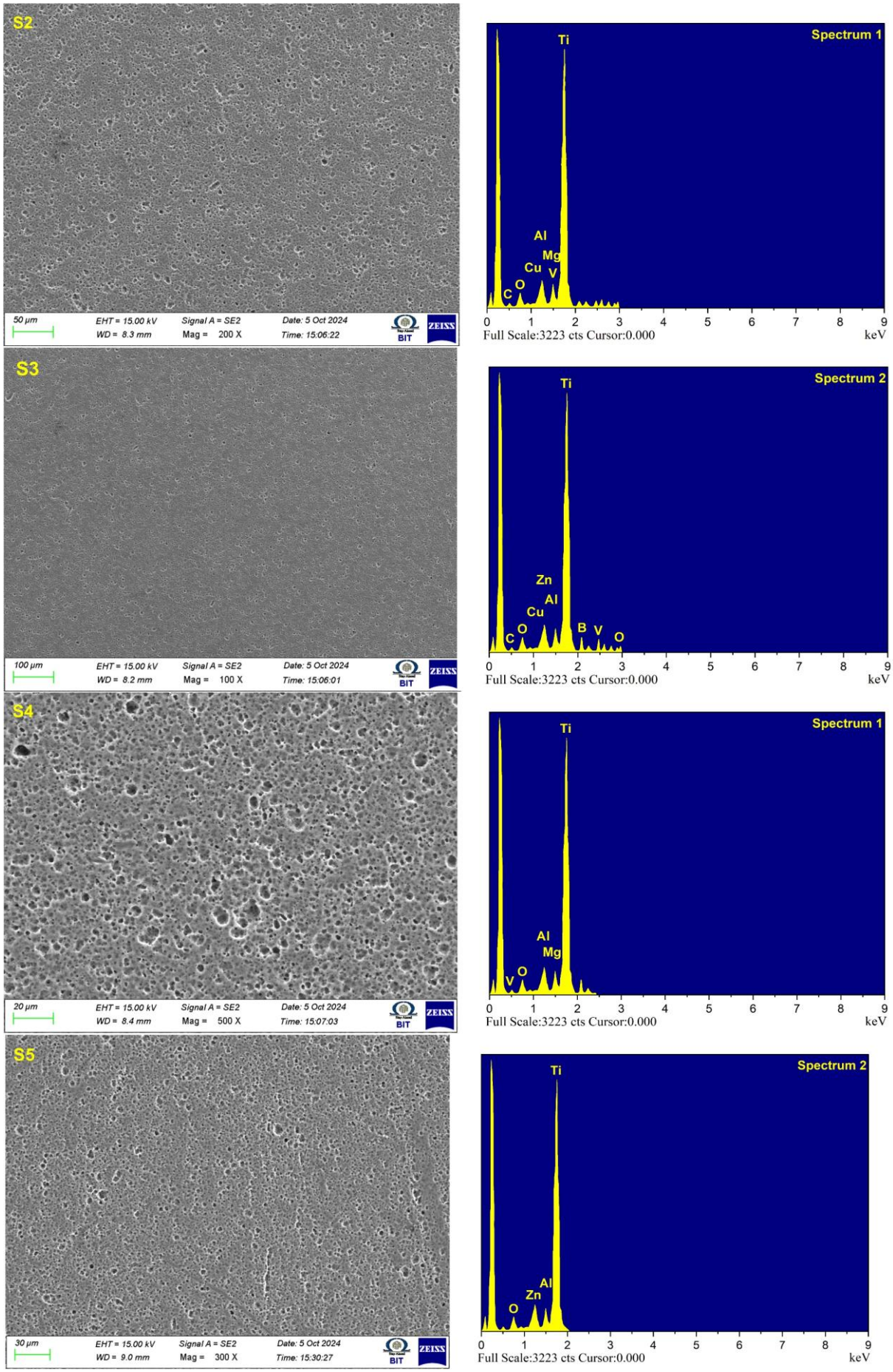

Fig. 10. Structural analysis of stir zone for samples S0 to S5 of SEM and EDS images

The enhanced wear resistance observed in the Ti-6Al-4V hybrid nanocomposites can be attributed to the synergistic interaction of the distinct reinforcement phases—TiC, ZrO_2, and graphite. TiC, with its high hardness, acts as a primary load-bearing phase, improving the load transfer efficiency and resisting deformation during sliding. ZrO_2 contributes through its superior toughness and chemical inertness, which promotes strong interfacial bonding with the Ti matrix, enhancing adhesion and reducing the likelihood of particle pull-out. Additionally, ZrO_2 particles contribute to Zener pinning, restricting grain growth during FSP and thereby contributing to microstructural refinement and increased hardness. Graphite plays a complementary role by forming a solid lubricating film at the sliding interface, which minimizes the direct contact between the pin and disc, thus reducing the coefficient of friction and wear loss. This film also fills micro-voids, reducing surface roughness and wear-induced crack initiation. SEM images (Figures 6, 8, 9, and 14) corroborate these mechanisms by showing well-dispersed reinforcement particles, minimal voids, and fine grain structures in the nugget zone. In particular, the worn surface of Sample 5 revealed minimal ploughing and smoother wear tracks, consistent with a lubricating graphite layer and strong interfacial bonding of ZrO_2. These combined mechanisms explain why Sample 5, containing 20%TiC + 60%ZrO_2 + 20%Gr, exhibited the lowest wear rate and COF, confirming a synergistic enhancement in tribological performance. While the SEM images confirmed uniform reinforcement dispersion and reduced cluster size after multiple FSP passes, quantitative grain size analysis was performed using the line-intercept method on etched SEM micrographs. The average grain size in the nugget zone was reduced from ~8–10 μm in the base alloy to ~2.1 μm after three FSP passes, indicating substantial grain refinement due to dynamic recrystallization. However, given Ti-6Al-4V's dual-phase (α+β) nature, localized transformation to β-phase or formation of fine acicular α may have occurred due to peak thermal cycles and severe plastic deformation during FSP. As an outcome of the substantial plastic deformation that occurs during friction stir processing, the reinforcing clusters shrink and break apart after three FSP passes. EDS and SEM images show that the reinforcement particles TiC, ZrO_2, and Gr are present and evenly distributed. However, the development of recrystallized crystals is impeded by the pinning effect of nanoscale reinforcements.

3.3. Microhardness Survey

The microhardness was evaluated along a horizontal line at 1 mm intervals, positioned 1mm beneath the upper surface of the NZ. Figure 11 illustrates the Vickers hardness values. The hardness of the 90% TiC reinforced sample 1s measured at 195 Hv, significantly higher than the base metal's hardness of 141 Hv. This is because the reinforcements are evenly distributed throughout the composite region. The maximal hardness values of hybrid samples 3, 4, and 5 are 189 Hv, 182 Hv, and 177 Hv, respectively. The reduction in hardness is attributable to the decreased percentage of TiC in the samples, which are 60%, 40%, and 20%, respectively. However, the 90% ZrO_2 reinforced sample 2 has a hardness value of 171 Hv, which is lesser than that of the other specimen but greater than that of the FSPed specimen, which has a hardness of 155 Hv without reinforcement. The FSPed sample demonstrates a higher level of hardness than the base metal as a consequence of grain refining. A substantial decrease in hardness was observed in the vicinity of the agitation zone, which was attributed to the reduced distribution of reinforcement components beyond this region. The hardness decreased in tandem with the base metal. The presence of nanoparticles promotes a fine grain structure, which in turn enhances hardness post-FSP. Because reinforcing particles are incorporated into the matrix, their grain boundary pinning action and stiff properties fortify the matrix. A rise in hardness range is attributed to the closure of microporosity, enhanced particulate dispersion, and substantial microstructural refinement that results from Friction Stir Processing (FSP). The FSPed composite achieved nearly double the microhardness and wear resistance due to microstructural refinement, martensite formation, and dispersion strengthening, while also slightly enhancing impact toughness [27].

In order to investigate the wear behavior of the samples, Figure 12(a) features a graph that illustrates the correlation between sliding distance and volume loss under a constant pressure of 20 N. The wear of all samples increases as the sliding distance increases, which is consistent with the results of previous investigations. This is a result of the metal matrix composites becoming

softer as a result of an increase in temperature with distance. Sample 3 composed of 60%TiC and 20% ZrO_2 reinforcement, demonstrates the least wear at shorter distances.

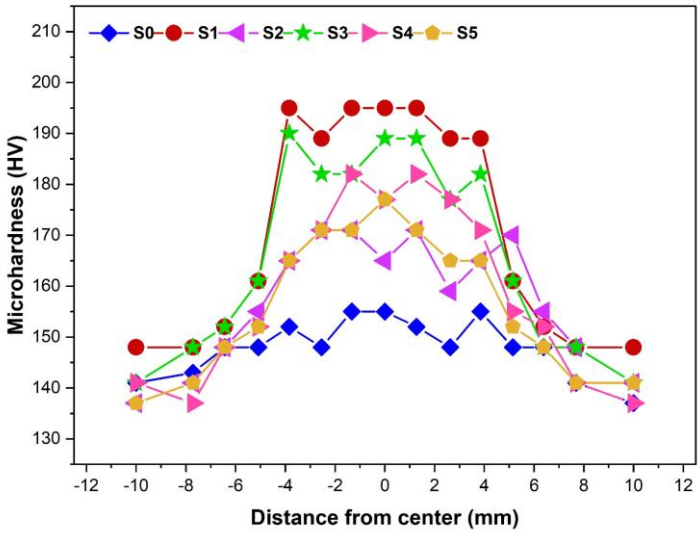

Fig. 11. Evaluation of Microhardness at stir zone for all samples

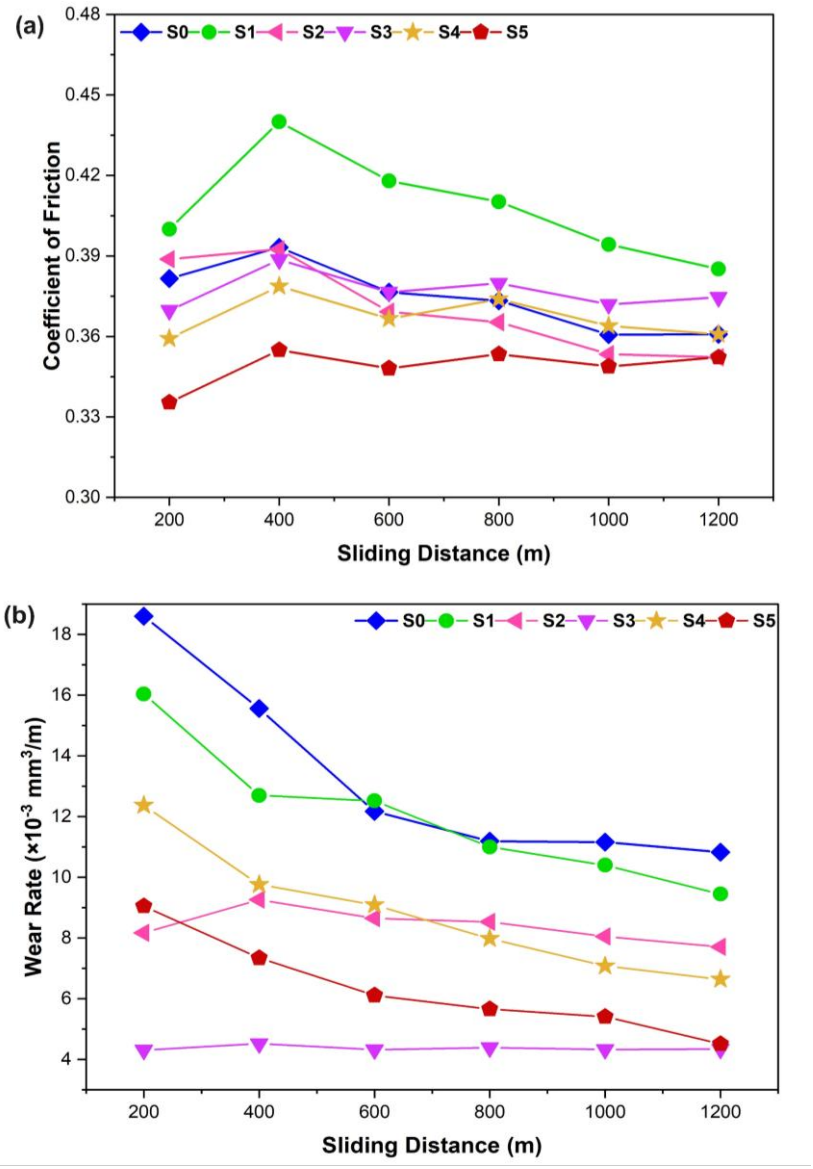

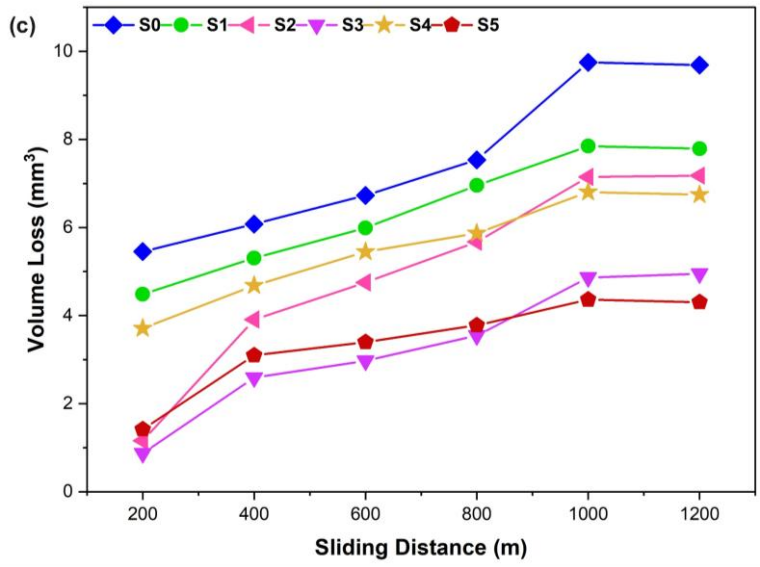

Fig. 12. (a) COF (b) Wear rate, (c) Volume loss of wear samples

However, as the sliding distance increases, Specimen 5 accomplishes minimal wear at a greater distance. FSPed sample 5 demonstrated a minimal volume loss of 4.884 mm^3, while the FSPed sample exhibited a maximal volume loss of 9.688 mm^3. The wear loss of the specimen 1 is composed of 80%TiC and 20% graphite, is 7.789 mm^3. Sample 3 showed a straight trajectory with negligible oscillations, with a wear rate of 0.0032 mm^3/m. On the other hand, as shown in Figure 12(b), sample 5 had the lowest wear rate of all the samples, going from 1.415 $mm^3\ m^{-1}$ to 1.160 $mm^3\ m^{-1}$. Because it has the lowest average coefficient of friction compared to the others, as seen in Figure 12(c). The surface hybrid nanocomposite's graphite particles create a cohesive layer between the disc and pin while they glide, reducing wear and acting as a lubricant. The FSPed layer showed a 25% increase in hardness and improved strength, ductility, and wear resistance compared to untreated alloy, with benefits attributed to dynamic and static recrystallization and spinodal decomposition [28].

During sliding, the wear rate gradually decreases as an outcome of the slow development of oxide in the contact zone between the disc and pin. A shear lag mechanism may have formed as a result of the micro/nano reinforcements spread out throughout the NZ, which served to reduce the applied load. Under shear stress, plastic is less prone to deformation and displacement. Similarly, the Orowan strengthening technique was successful. Friction stir processing increases wear resistance and durability by reducing plastic deformation and forming numerous dislocations around reinforcement particles due to the variations in thermal expansion coefficients among the matrix and the reinforcements during solidification. This reinforcing mechanism is made feasible by the process of work hardening.

The coarse powder particles were unable to adhere to the material flow induced by the tool, resulting in a tenuous contact between the micro-sized TiC hard particles and the matrix. The reinforcement particle ratio (20%TiC + 60 %ZrO_2 + 20% Gr) in Sample 5 is responsible for its exceptional wear resistance. A hybrid nano surface composite is formed when nano ZrO_2, micro-TiC, and Gr bind strongly to the matrix. In order to create a strongly bound matrix, the processing tool uses tiny, fine-grained ZrO_2 particles to outline the plastic flow of the material.

Figure 13 depicts the pin-disc coefficient of friction (COF). The first spike in COF is produced by the friction force needed to improve the adhesive among the sample POD. In the initial phase of sliding, the ordinary friction stir processed (FSPed) sample exhibits a substantial fluctuation in the COF. The presence of strong alloying elements in the base metal interacting with the worn surface could be the cause of this oscillation (Fig 13 (a)). Variations in the COF graph were caused by the wear process, which created and removed the worn surface layer.

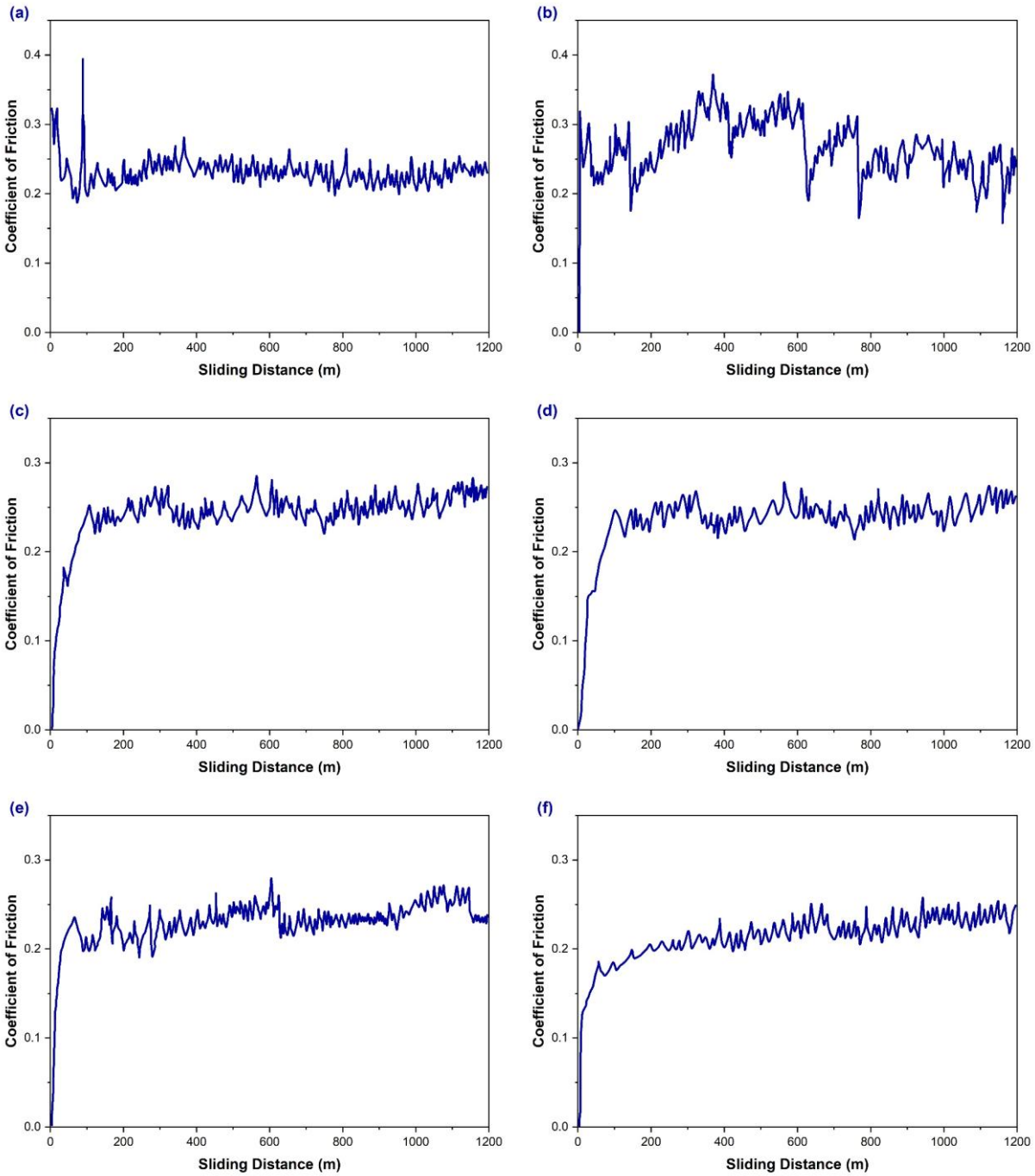

Fig. 13. COF plot of sample S0 to S5

The sample 1 possess exhibited a COF pattern that was gradually revealed (Figure 13 (b)). The coefficient of friction (COF) reaches a zenith at each stage, followed by a sudden decline, which is followed by a brief period before rising again for the next stage. This can be attributed to the increased ratio of TiC, which impedes movement to some degree and separates from the surface, resulting in abrasion. Sample 2 has an elevated coefficient of friction (COF) at the commencement of sliding, averaging 0.3653, which then diminishes to 0.3534 in the later phases, accompanied by slight fluctuations (Figure 13 (c)). The enhanced binding strength with the base matrix is a result of the higher proportion of nano ZrO_2.

Sample 3 contains 60%TiC and 20% ZrO_2, exhibits protracted phases of coefficient of friction (COF) with reduced fluctuations, resulting in mean value of 0.3746, which is lower than the 0.3851 COF of sample 1, in contrast to sample 1, which contains 80%TiC (Figure 13 (d)). This may be due to the motion resistance that TiC maintains over a longer distance as a result of the incorporation of ZrO_2. The increased stage distance of COF in sample 4 is also a result of a greater ZrO_2 concentration in

the hybridized strengthening particle ratio (Figure 13 (e)). The mean COF value is 0.3816, which is less than sample 3's value. Starting at 0.3354 at the beginning of the sliding distance and experiencing mild changes, the coefficient of friction (COF) for sample 5 eventually climbs to 0.3552 with somewhat increasing volatility. However, when compared to all other COF plot, specimen 5 had the lowest average value and the fewest oscillations (Figure 13 (f)).

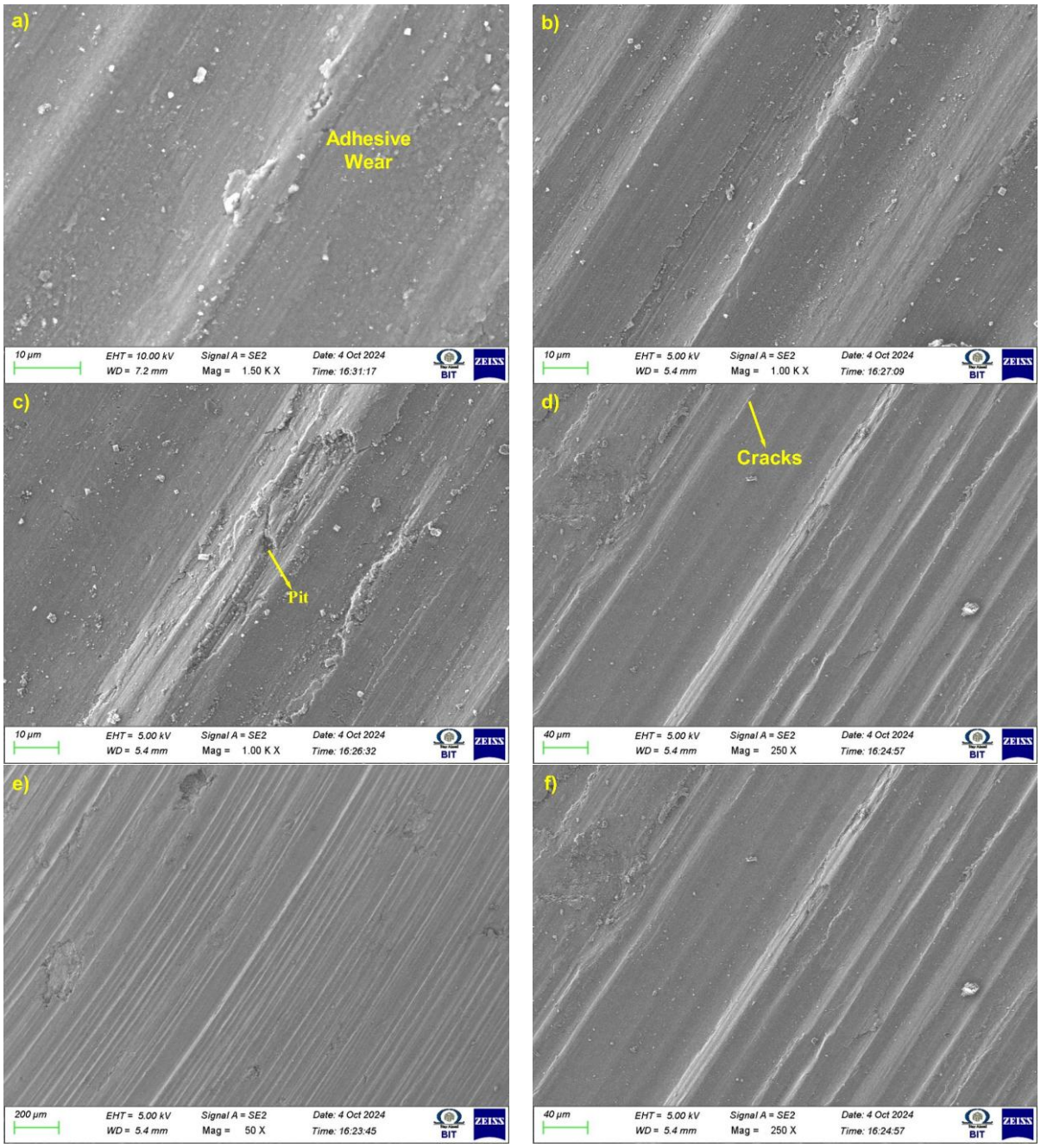

Fig. 14. Microstructure of wear analysis for samples S0 to S5

Figure 14 shows the SEM image of the worn-out surface show that the friction stirs processing sample without reinforcing particles has adhesive wear and an increased COF in its eroded surface and wear formation. The specimen with 80% TiC and 20% Gr shows a wear loss of 6.3124 mm^3 compared to the simple friction stir processed sample, since it contains the most titanium carbide reinforcement (Figure. 14a). The entrapment of TiC particles between contact surfaces resulting from the detachment of TiC particles from the composite during wear progression elevates the COF and exacerbates abrasive wear. The abrasive wear of sample 2, resulting from the ongoing production and removal of the hard layer (Figure. 14b). Figure 14c, d show that the surface layer of samples 3 and 4 ruptured due to several perpendicular cracks on their degraded surfaces. There was also delamination and abrasive wear. Figure 14f demonstrate the degraded morphological

analysis of Specimen 5, which reveals a defect free track with minimal surface flaws. When compared to the other samples, its deterioration is almost nonexistent. A combination of nano-sized ZrO_2 particles and rigid micro-sized TiC particles creates a pinning effect that greatly adheres to the matrix, providing wear resistance. The presence of pores highlighted the impact of microstructure on wear properties [29].

3.5. Wear Optimization Using RSM

It is the goal of the optimize to recognize the input factors that prevent degradation. Table 7 shows the input parameter ranges and the accompanying responses for the desirability analysis. A weight of 1 and an equal significance of 3 are ascribed to all parameters..

Table 7. Results on desirability analysis.

Factors	Goal	Min limit	Max limit
A (%)		20	60
B (N)	In range	25	45
C (ms^{-1})		1	1.6
Wear (mm^3)	Minimum	6.11	10.08

With a load of 26.5267 N and a velocity of 1.0048 m/s, the optimal solution is shown in Figure 15, which also shows that ZrO_2 is at 59.9433%. The ideal settings for input and response predictions on the ramp graph, indicated by the dot. Twenty solutions were generated by the study, and the one with the highest attractiveness score of 1.000 was selected. Comparisons were made between the expected values from the response surface model and the experimental values from hybrid nanocomposites that were made with a certain amount of reinforcement mixtures under ideal conditions

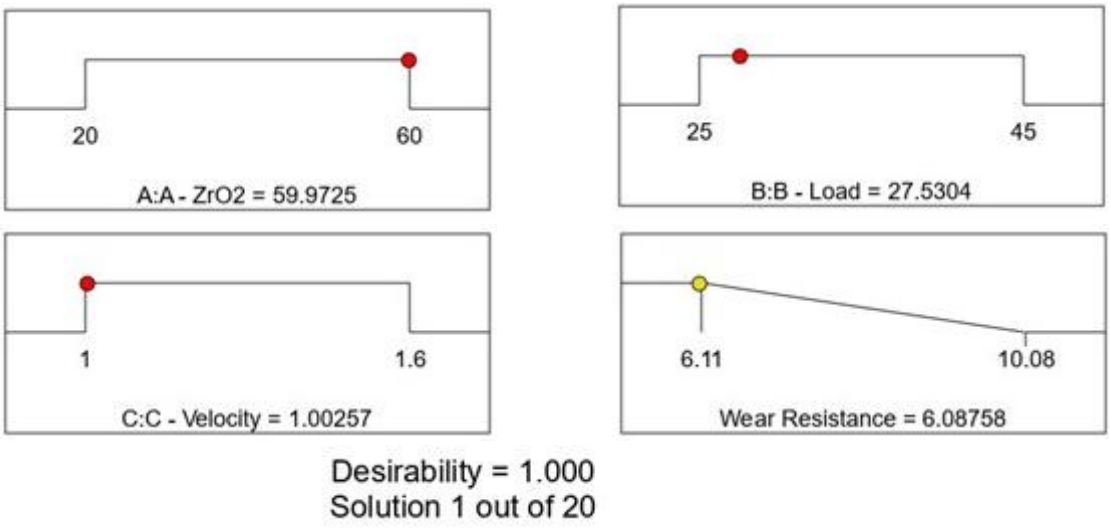

Fig. 15. Desirability plot for wear

Table 8. Evaluation of predicted and experimented values for wear.

Specimen code	Predicted (mm^3)	Experimented (mm^3)	Error (%)
S4	6.56	6.52	0.613
S5	8.6	8.5	1.176
S6	5.98	6.11	-2.128

Table 8 presents a comparison of the actual and anticipated values for a wear measurement of 6.05441 mm^3. The maximum percentage error is -2.128, signifying that the developed model precisely forecasts the actual data. The study employed ANOVA and RSM for developing semi-empirical correlations of machining indices [30].

The tribological characteristics of the engineered Ti-6Al-4V surface hybrid nanocomposite are explained in relation to the influence of TiC/ZrO_2 in conjunction with graphite particles. The incorporation of reinforcing particles results in a substantial increase in the microhardness of the synthesized composites, reaching a maximal of 184 Hv. The composite containing the highest TiC and the lowest ZrO_2, while maintaining a constant graphite content, demonstrates minimal wear at reduced sliding distances; nevertheless, due to abrasive and delamination wear mechanisms, the wear volume escalates over increased sliding distances. The composite containing the highest ZrO_2 and the lowest TiC, with a consistent quantity of graphite, demonstrates the minimal volume loss at increased sliding distances owing to the lowest average COF. The pinning and lubricating effects of the augmented presence of nanosized ZrO_2, in conjunction with TiC and graphite particles, are responsible for the wear resistance. These particles demonstrate strong adhesion to the matrix. Table 9 shows the comparative analysis of the prior study and with this study.

Table 9. Comparative analysis

Composite System	Hardness (Hv)	Wear Loss (mm^3)	COF (Avg)	Reference
Ti-6Al-4V+SiC/TiB2(FSP)	185-195	5.8	0.31	[7]
Ti-6Al-4V+SiC (Laser Clad)	180	6.5	0.35	[20]
Ti-6Al-4V+ZrO_2 +Gr (This study, Sample 5)	177	4.88	0.1793	Present Study

The observed improvement in wear performance is consistent with the findings reported by author [5], where Ti-6Al-4V reinforced with TiC and B_4C through friction stir processing (FSP) exhibited enhanced wear resistance due to grain refinement and second-phase dispersion strengthening. Similarly, researchers [18] demonstrated that laser-clad coatings with Ni-coated graphite on Ti alloys significantly reduced wear due to the formation of a lubricating tribolayer. The hybrid reinforcement used in the present study offers a unique balance: TiC provides load-bearing capability and high hardness, ZrO_2 contributes toughness and crack deflection, and graphite reduces interfacial shear through tribofilm formation. These mechanisms collectively reduce adhesive and abrasive wear, as confirmed by smoother wear tracks and lower coefficient of friction in Sample 5. Unlike prior studies that used only single-phase reinforcements, the current multi-phase system shows improved synergy, yielding up to 49.6% reduction in wear and 53.5% reduction in COF relative to the unreinforced sample. The effectiveness of multi-pass FSP further promotes particle distribution uniformity, which is crucial for minimizing localized stress concentrations and particle pull-out—both major contributors to wear degradation.

4. Conclusions

This study demonstrates the successful fabrication of a hybrid surface nanocomposite on a Ti-6Al-4V alloy using Friction Stir Processing (FSP), incorporating titanium carbide (TiC), zirconium oxide (ZrO_2), and graphite (Gr) as reinforcements. The process parameters—750 rpm rotational speed, 20 mm/min traverse speed, and a tool tilt angle of 3°—were optimized to achieve a homogenous dispersion of reinforcements. The unique approach of embedding reinforcement mixtures in multiple, uniformly spaced holes prior to processing ensured consistent distribution and strong metallurgical bonding throughout the stir zone. The hybrid nanocomposite exhibited substantial improvements in mechanical and tribological properties compared to the unreinforced and conventionally FSPed Ti-6Al-4V alloy. Microstructural analysis confirmed a uniform dispersion of reinforcing particles and refinement of grain structures, contributing directly to enhanced hardness and wear resistance. Among the studied compositions, the sample reinforced with 30% TiC, 60% ZrO_2, and 10% Gr demonstrated superior performance, exhibiting a peak hardness of 191 Hv—considerably higher than the 149 Hv of the FSPed base alloy. Additionally, this composition minimized wear loss to 2.9526 mm^3 and achieved the lowest mean coefficient of friction (0.1793), signifying an optimal balance between hard and lubricating phases. The reinforcement synergy

played a critical role in enhancing composite performance. TiC contributed high hardness and load-bearing capability, ZrO_2 improved toughness and structural stability, while graphite acted as a solid lubricant, reducing friction and wear. The combined effect of these reinforcements led to a pronounced reduction in adhesive and abrasive wear mechanisms, as observed from wear track morphology. From a practical perspective, the proposed hybrid composite offers excellent potential for applications in aerospace, automotive, and biomedical sectors where enhanced wear resistance, surface hardness, and material integrity are critical. Furthermore, the scalability and energy efficiency of the FSP technique make it suitable for industrial adoption. This research thus provides a valuable pathway for the development of multifunctional, high-performance titanium-based surface composites.

Friction stir processing (FSP) offers significant microstructural refinement and superior wear resistance, but its industrial scalability poses certain challenges. The process requires precise fixturing, custom tool design (especially for reactive alloys like Ti-6Al-4V), and multiple passes for uniform reinforcement distribution—leading to increased processing time and operational complexity. Compared to laser cladding and PTA welding, FSP is a solid-state process that eliminates solidification defects and results in superior mechanical bonding with fewer residual stresses. However, laser cladding is faster for large areas and is more adaptable to automated systems, while PTA welding allows deeper material penetration. From a cost standpoint, FSP is economically viable for small-to-medium-scale applications requiring high precision and localized enhancement (e.g., aerospace fastener zones, biomedical implants), but less so for mass production. Scaling FSP for large components requires integration with CNC-controlled setups or robotic arms, which increases initial capital costs. Future work should focus on developing continuous or high-speed FSP variants, incorporating real-time process monitoring, and exploring cost–benefit trade-offs for broader industrial deployment.

References

[1] Alam ST, Amin AN, Hossain MI, Huq M, Tamim SH. Performance evaluation of graphite and titanium oxide powder mixed dielectric for electric discharge machining of Ti-6Al-4V. SN Appl Sci. 2021;3(4). https://doi.org/10.1007/s42452-021-04450-6

[2] Shi B, Huang S, Zhu P, Xu C, Guo P, Fu Y. In-situ TiN reinforced composite coatings prepared by plasma spray welding on Ti6Al4V. Mater Lett. 2020;276:128093. https://doi.org/10.1016/j.matlet.2020.128093

[3] Jeyaprakash N, Prabu G, Yang CH. Formation of different phases and their influences on the mechanical and tribological properties of surface alloyed FeCoCrNiAl particles using PTA technique. Intermetallics. 2022;142:107457. https://doi.org/10.1016/j.intermet.2021.107457

[4] Sahai RSN, Jadhav PN, Raut AS, Surve SS. Study on performance of multiwall carbon nanotubes and functionalized multiwall carbon nanotubes/poly aryl ether ketone polymer composite gears. Res Eng Struct Mater. 2025;11(1):273-85. http://dx.doi.org/10.17515/resm2024.217na0324rs

[5] Dahiya MS, Gupta M. Optimization of process parameter of FS-welding of aluminum-lithium alloy (AA8090) by using desirability analysis. Res Eng Struct Mater. 2025;11(2):607-30. http://dx.doi.org/10.17515/resm2024.275ma0511rs

[6] Tarasov S, et al. Friction stir welding of Ti-6Al-4V using a liquid-cooled nickel superalloy tool. Technologies (Basel). 2022;10(6). https://doi.org/10.3390/technologies10060118

[7] Deore HA, Nichul U, Rao AG, Hiwarkar VD. Influence of SiC particles and post-heat treatment on the properties of Ti-6Al-4V-based surface nanocomposite fabricated by friction stir processing. Surf Coat Technol. 2022;449:129002. https://doi.org/10.1016/j.surfcoat.2022.128985

[8] Adetunla A, Akinlabi E, Jen TC. In-depth characterization of FSP-enhanced aluminum metal matrix: A study in materials modeling and computational techniques. J Mater Res Technol. 2024;29:5721-30. https://doi.org/10.1016/j.jmrt.2024.02.229

[9] Deore HA, Mishra J, Rao AG, Bhanushali BD, Hiwarkar VD. Utilizing additive friction stir processing to fabricate B4C reinforced Ti-6Al-4V matrix surface composite: Microstructure refinement and enhancement in mechanical properties. Met Mater Int. 2022;28(1):322-35. https://doi.org/10.1007/s12540-021-01094-4

[10] Zhang W, Liu H, Ding H, Fujii H. Superplastic deformation mechanism of the friction stir processed fully lamellar Ti-6Al-4V alloy. Mater Sci Eng A. 2020;785:139379. https://doi.org/10.1016/j.msea.2020.139390

[11] Kalashnikova TA, Cheremnov AM, Eliseev AA, Gurianov DA, Kalashnikov KN. Features of the material structure in the tool effect area during friction stir processing of additively manufactured Ti-6Al-4V alloy workpieces. AIP Conf Proc. 2023;2803:030011. https://doi.org/10.1063/5.0169803
[12] Kalashnikov K, et al. Friction stir processing of additively manufactured Ti-6Al-4V alloy: Structure modification and mechanical properties. Metals (Basel). 2022;12(1):86. https://doi.org/10.3390/met12010055
[13] Geyer M, Avettand-Fènoël MN, Vidal V, Rezaï-Aria F, Boher C. Multi-scale effects of the tool shape and length on the interfacial microstructure and the mechanical behaviour of Al2024/Ti-6Al-4V lap friction stir welds. J Manuf Process. 2024;113:360-72. https://doi.org/10.1016/j.jmapro.2024.01.056
[14] Zhang L, Long W, Du D, Wu Q, Jiang C. The microstructure and wear properties of diamond composite coatings on TC4 made by induction brazing. Diam Relat Mater. 2022;125:108568. https://doi.org/10.1016/j.diamond.2022.109032
[15] Srinivasan D, Sevvel P, Dhanesh Babu SD, Roy V. Optimization of parameters and formulation of numerical model employing GRA-PCA and RSM approach for friction stir welded Ti-6Al-4V alloy joints. Mater Res Express. 2024;11(5):056523. https://doi.org/10.1088/2053-1591/ad48e3
[16] Perumal G, Senthilkumar N, Satheshkumar D, Anandhakumar S. Comparative analysis of solution treatment with short and long-term aging on mechanical, tribological, and corrosion potential of Ti-6Al-4V alloy. Multiscale Multidiscip Model Exp Des. 2025;8(3):357-72. https://doi.org/10.1007/s41939-025-00759-6
[17] Kumar PSSR, Mashinini PM. Friction stir welding characteristics of dissimilar/similar Ti-6Al-4V-based alloy and its machine learning techniques. In: Advanced Joining Technologies. 2024. p. 227-44. https://doi.org/10.1201/9781003327769-13
[18] Perumal G, Senthilkumar N, Naik N, Deepanraj B. Comparative assessment of the mechanical, tribological, and corrosion properties of Al/SiC/Al2O3 and Al/SiC/TiO2 hybrid composites. Discov Appl Sci. 2025;7(4):148. https://doi.org/10.1007/s42452-025-06687-x
[19] Prabakaran T, Kumar DR, Vijayan K, Ganesh KMM, Thamizhvalavan P. An investigation on microstructures, mechanical and wear behavior of laser-cladded Inconel 625 and Nimonic 90 over Nimonic 90 substrate. Surf Rev Lett. 2024;31(5):2250074. https://doi.org/10.1142/S0218625X24500380
[20] Yu H, Lu L, Wang Z, Chen C. Microstructure and wear resistance of a composite coating prepared by laser alloying with Ni-coated graphite on Ti-6Al-4V alloy. Materials (Basel). 2022;15(16):5556. https://doi.org/10.3390/ma15165512
[21] Zhang Z, et al. Influence of welding distance on tool wear in friction stir welding of Ti-6Al-4V alloy. Rare Met Mater Eng. 2023;52(7):2525-32.
[22] Yu H, Meng X, Wang Z, Chen C. Influence of scanning speed on the microstructure and wear resistance of laser alloying coatings on Ti-6Al-4V substrate. Materials (Basel). 2022;15(17):5966. https://doi.org/10.3390/ma15175819
[23] Prabu G, Duraiselvam M. Tribological studies on AlCrFeCuCoNi high entropy alloy surface coated on Ti-6Al-4V using plasma transferred arc technique. Arch Metall Mater. 2022;67(2):409-20. https://doi.org/10.24425/amm.2022.137772
[24] Venkatesh BN, Hebbal U, Siddappa PN, Kousik S, Nagaraja TK. Optimization of FSW parameters of AA6061-6 wt.% SiC composite plates. Manuf Rev (Les Ulis). 2022;9:16. https://doi.org/10.1051/mfreview/2022032
[25] Zykova A, et al. In situ intermetallics-reinforced composite prepared using multi-pass friction stir processing of copper powder on a Ti6Al4V alloy. Materials (Basel). 2022;15(7):2550. https://doi.org/10.3390/ma15072428
[26] Ehsan S, Khan SA, Rehman M. Defect-free high-feed milling of Ti-6Al-4V alloy via a combination of cutting and wiper inserts. Int J Adv Manuf Technol. 2021;114(1-2):641-53. https://doi.org/10.1007/s00170-021-06875-0
[27] Deore HA, Nichul U, Rao AG, Hiwarkar VD. Microstructural investigation of WC reinforced Ti-6Al-4V matrix surface composite fabricated via additive friction stir processing. Materialia. 2021;20:101208. https://doi.org/10.1016/j.mtla.2021.101235
[28] Zykova AP, et al. The influence of multipass friction stir processing on formation of microstructure and mechanical properties of Ti6Al4V alloy. Russ J Non-Ferr Met. 2022;63(2):167-76. https://doi.org/10.3103/S1067821222020146
[29] Su ML, Li JN, Shan FH, Liu KG, Xu HL. Microstructure performance of La2O3-modified tungsten inert gas clad composite coating. Surf Rev Lett. 2020;27(7):1950166. https://doi.org/10.1142/S0218625X19501828
[30] Karmiris-Obratański P, Papazoglou EL, Leszczyńska-Madej B, Zagórski K, Markopoulos AP. Surface and subsurface quality of titanium grade 23 machined by electro discharge machining. Materials (Basel). 2022;15(1):46. https://doi.org/10.3390/ma15010164